Postprint of: Wołoszyk K., Garbatov Y., Kowalski J., Indoor accelerated controlled corrosion degradation test of small- and large-scale specimens, OCEAN ENGINEERING, Vol. 241 (2021), 110039, DOI: 10.1016/j.oceaneng.2021.110039



# Indoor accelerated controlled corrosion degradation test of small- and large-scale specimens

**Krzysztof Woloszyk [1], Yordan Garbatov [2,*] and Jakub Kowalski [1]**

[1]Institute of Naval Architecture and Ocean Engineering, Gdansk University of Technology, G. Narutowicza 11/12 st., 80-233 Gdansk, Poland; krzwolos@pg.edu.pl

[2]Centre for Marine Technology and Ocean Engineering (CENTEC), Instituto Superior Técnico, Universidade de Lisboa, Avenida Rovisco Pais 1049-001 Lisboa, Portugal; yordan.garbatov@tecnico.ulisboa.pt

*Correspondence: yordan.garbatov@tecnico.ulisboa.pt; Tel.: (351) 21 841 7907

**Abstract:** The work presented here is a part of a long-term project analysing the structural behaviour of ageing marine structures. An accelerated corrosion degradation set-up was developed to reproduce specimens of corroded marine structural specimens of different degrees of degradation, controlling various natural factors, *i.e.*, temperature, oxygen content, salinity, and flow velocity. The nine stiffened plates of 1.2 m length and 30 small scale specimens made of mild steel of three different thicknesses have been corroded. The mean corrosion depth and rate have been controlled during the degradation process for all specimens. The corrosion degradation characteristics have been measured and analysed. In the case of small-scale specimens, microscope scanning, and for the stiffened plates, ultrasonic thickness measurements were performed. The obtained corrosion surfaces are highly non-uniform. During the corrosion degradation, a number of measurements were performed to satisfy a confidence level of 95% and an error of 10%. The developed corrosion degradation is compared with a real corrosion depth measurement of ship deck plates of ballast and cargo tanks, showing a very good similarity in the trend and the corrosion acceleration, concluding that the developed corrosion degradation controlled experimental set-up is efficient in reproducing marine structural specimens of different degree of degradation for further mechanical testing.

**Keywords:** corrosion testing; marine; stiffened plates; specimens

## 1. Introduction

The corrosion degradation tests are needed as a part of the evaluation process of the structural behaviour of ageing structures, such as ships and offshore structures (Garbatov et al., 2018, 2017; Saad-Eldeen et al., 2013). There are various methods to achieve the corroded state of the structural components. The in-situ corrosion degradation tests are recommended since the real corrosion conditions could be captured. The examples of such tests may be found (Zakowski et al., 2014; Zhu et al., 2020), where specimens were tested in sea conditions. However, significant corrosion degradation levels are achieved in ship structures after around 12-15 years (Garbatov et al., 2007). Based on the measurement of real corrosion degradation, various corrosion models have been developed, e.g., Melchers (2008, 1999); Yamamoto and Ikegami (1998); Guedes Soares and Garbatov (1999, 1998); Paik et al. (1998); Qin and Cui (2003). Apart from the long duration of the in-situ corrosion tests, one cannot accurately control the structural component corrosion degradation level. This applies to components taken from operating structures and the ones intentionally fabricated and left in the sea. Since the corrosion degradation is subjected to significant scatter (Melchers, 1999), the estimation of corrosion degradation test duration to achieve the assumed level of degradation is very challenging. In laboratory conditions, the periodical measurements of the corrosion degradation levels are much easier to be done.

When the precise corrosion degradation rate is not the main objective of the corrosion testing, but the achievement of the specific level of degradation (mean percentage reduction of the plate thickness), the laboratory testing seems more suitable. This is the case when one wants to investigate the influence of corrosion degradation on the behaviour of the structures. Further, to accelerate the corrosion process,

the proper conditions need to be created. The testing procedures are already well developed for small-scale specimens (Baboian, 2005), considering different corrosion types, *i.e.* atmospheric, marine immersed, etc. Examples of such testing could be found very often, and there are performed for various applications (Chen et al., 2021; Nie et al., 2019; Orlikowski et al., 2017; Xu et al., 2019). These applications include estimating the corrosion rate in a particular environment, validating new methods for measuring the corrosion characteristics, and investigating the mechanical properties of corroded metals. However, considering large-scale specimens, such as beams or plates, the existing guidelines are relatively modest (ASTM Norma G 52, 2006).

Nevertheless, some examples of such tests could also be found, but there are relatively rare when compared to tests performed on a small scale. P. Domzalicki, I. Skalski, C. Guedes Soares (2009) performed the marine immersed corrosion tests for box girders, simulating the ship hull girder. In this case, the specimens were submerged near the harbour and corrosion was accelerated using electric current. Wang et al. (2020) presented the tests of steel beams subjected to atmospheric corrosion and subjected to a bending load. Finally, the atmospheric corrosion tests of corroded box girders were given (Jin et al., 2020), representing the typical bridge structure.

One of the most critical problems in accelerated corrosion degradation testing is achieving similar characteristics of the corroded structural specimens. Xiao et al. (2020) has shown that when specimens are corroded with the DC power input source application, the corrosion morphology will be different from those obtained in natural conditions. Natural conditions will bring higher non-uniformity in thickness distribution. The structural behaviour will be other too. Thus, only changing the natural factors that influence corrosion rate should be controlled, *i.e.* physical, chemical and biological (Pedeferri, 2018).

In the study presented by Woloszyk and Garbatov (2021), the experimental set-up for marine immersed corrosion has been developed to test the large-scale specimens in accelerated conditions. The approach is economically efficient since all equipment pieces are not expensive compared to the available commercial solutions. The corrosion degradation has been accelerated by reaching the optimum salinity level and increasing the oxygen content, temperature, and water circulation. Thus, only natural factors have been governed, avoiding accelerating the corrosion process electrically.

Although the current study is devoted to the testing of plates, the studies performed regarding corroding bars in steel-reinforced concrete shown that from various acceleration corroding techniques, the one that avoids applying electric current and only alternates climatic conditions, are most likely to reproduce the natural process of ions transport. Yuan et al. (2007) stated that the uneven corrosion distribution on the steel bar surface will be obtained for the method, where only natural factors are controlled. Thus, despite differences between corrosion of bars and plates, controlling only natural factors will lead to similar conditions in a real sea environment. The corrosion testing aimed to corrode specimens for future strength testing. Therefore, it has been more oriented toward engineering applications.

The current study develops an accelerated controlled marine immersed corrosion set-up to corrode small-scale specimens, and larger-scale stiffened plates. The small-scale specimens are considered of significantly smaller size regarding the real structure, which can be used to determine, e.g., mechanical properties. However, large-scale specimens are considered a part of real structure, eventually of slightly lower scale, used to assess structural behaviour of such components (e.g., beams, plates, girders). The tests have been performed using the experimental set-up as presented by Woloszyk and Garbatov (2021), and the set-up information has been provided in the following sections. The corrosion degradation was monitored during testing. The change of mean corrosion depth was estimated and fitted to multi-stage regression equations representing a specific confidence and error level of measurements. In addition, all relevant corrosion characteristics, such as mean value thickness and standard deviation and corrosion depth distribution within specimens, were analysed.

## 2. Specimens

The specimens subjected to the corrosion degradation process are stiffened plates of a 1.2m length and 0.4 m width with a stiffener of a 0.1 m height, made from normal strength steel of S235. Three different thicknesses were investigated: 5, 6 and 8 mm. The chemical composition of each plate, as defined by the manufacturer, is presented in Table 1. The total number of nine specimens was tested, three specimens for each thickness. The specimens were automatically welded, and more details regarding welding procedure and residual stresses may be found in (Woloszyk et al., 2020). After welding, the faces of welds were ground.

**Table 1.** Chemical composition of tested steel specimens.

| Thickness [mm] | Fe [%] | C [%] | Si [%] | Mn [%] | S [%] | P [%] | Cu [%] | Al [%] | N [%] |
|---|---|---|---|---|---|---|---|---|---|
| 5 | 99.2 | 0.1 | 0.01 | 0.48 | 0.013 | 0.025 | 0.04 | 0.03 | 0.004 |
| 6 | 99.1 | 0.12 | 0.03 | 0.51 | 0.011 | 0.015 | 0.06 | 0.03 | 0.004 |
| 8 | 99.0 | 0.13 | 0.024 | 0.67 | 0.012 | 0.023 | 0.026 | 0.03 | 0.004 |

Additionally, the total number of 30 standard specimens (fabricated according to the ISO norm (ISO, 2009)) was corroded, with a total length of 250 mm and a total width of 60 mm, and a gauge section of 110 mm x 40 mm.

### 3. Experimental set-up

The corrosion test set-up has been already presented in (Woloszyk and Garbatov, 2021). Thus, only the main features are presented herein. A 900-litre tank made from GRP laminate has been chosen for this purpose. Figure 1 (right) shows the set-up with the big-scale specimens placed alongside and small-scale coupon specimens placed on the supporting structure.

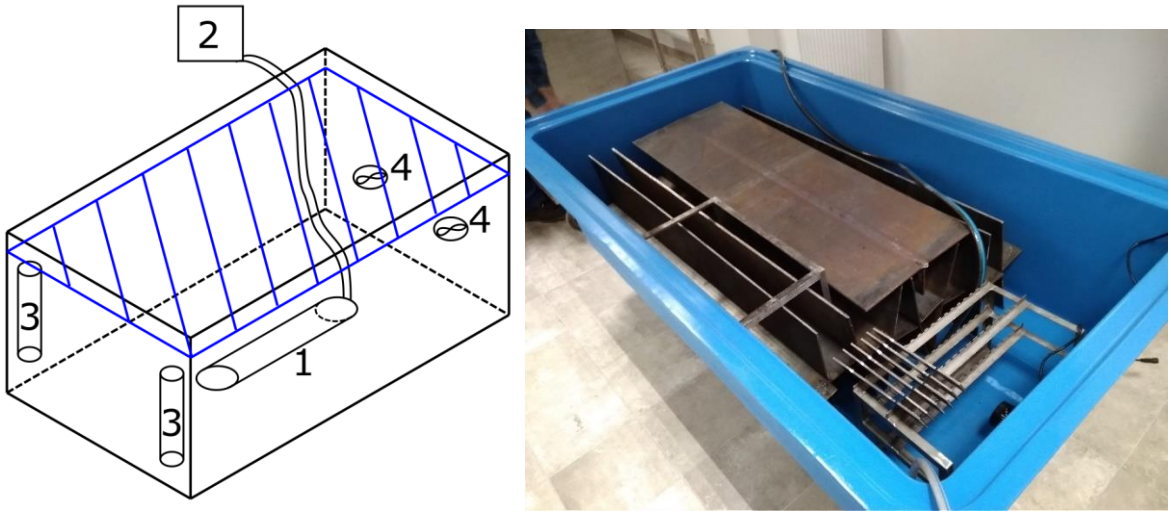


(**a**) (**b**)

**Figure 1.** The used equipment (1- linear diffuser, 2 – aeration pump, 3 - heaters, 4 – circulation pumps) (a) and corrosion tank with placed specimens (b) (Woloszyk and Garbatov, 2021).

The generic scheme of the used equipment in the tank is presented in Figure 1 (left). The aeration pump (2) of efficiency equal to 40 $m^3/h$ has been used to increase the oxygen content in the water. The additional air has been pumped into the water through the linear diffuser (1). The application of circulation pumps (4) has provided water circulation, and the heaters covered by a glass shell (3) controlled the water temperature. Two heaters of a total power of 800 W have been used for automatic stabilisation of the temperature. The optimum salinity (35 ppm) has been established. The freshwater

has been mixed with the natural salt (obtained by the evaporation of the actual sea water), which led to the artificial seawater free of microbiological components. It needs to be highlighted that in real marine immersed corrosion, microorganisms could change the corrosion characteristics. However, this factor is tough to be simulated in laboratory conditions and controlling this factor will be very challenging. This could lead to an additional spread in the corrosion rates and thickness distributions in the specimens. Thus, to avoid that, the microorganisms were not considered in this study.

Further, the forced current could interact with the microorganisms. In laboratory simulation without microorganisms, oxygen concentration and flow velocity changes will not significantly impact corrosion morphology, although some influence could occur. During corrosion testing, the water has been twice replaced to remove a significant amount of corrosion products. The assumed governing factors were temperature of 35 °C, 300% oxygen content concerning supersaturation conditions, and a water speed of 0.03 m/s. Henry's law gives the oxygen content of any liquid at a particular temperature. However, a much higher gas concentration level is possible, even at atmospheric pressure, if the gas is additionally applied to the solution. Because diffusional escape of gas across the solution may be slow compared to the gas input rate, the supersaturation conditions could be easily achieved, leading to metastable equilibrium. According to Bowers et al. (1995), when oxygen is generated chemically, dissolved oxygen concentration could be 100 times the equilibrium solubility in atmospheric pressure. In the case of an aeration pump, such magnification is non-reachable (Colt and Westers, 1982).

Nevertheless, in the case of aeration (Yamashita and Ando, 2017), the supersaturation conditions reaching 600% has been achieved. Pedeferri (2018) proposed the equation for estimation of corrosion rate, based on the values of the governing parameters. The corrosion rate could be estimated as a function of the governing parameters, *i.e.*, temperature, oxygen content and flow velocity. The estimated corrosion rate in accelerated conditions was calculated as 0.736 mm/year for the variables' initially assumed values. The target corrosion level was considered equal to 21% of the specimen's initial mass (Degree of Degradation level) for the most severely corroded specimens.

The total duration of the corrosion test was 428 days. The corrosion testing aims to produce corroded samples with a specific degree of degradation of an acceptable confidence level within a specified time frame instead of long-lasting corrosion testing.

Thus, during the design of the corrosion test set-up (Woloszyk and Garbatov, 2021), the corrosion degradation rate was performed, and some measure was carried out to fit with the planned period of corrosion tests. Several possible approaches to increase the corrosion degradation rate were available. The oxygen content measurements were carried out, showing that the approximated level of supersaturation has been lower than the assumed one and was closer to 200%. Additionally, the accelerated corrosion deterioration testing of plates, using the engineering experimental set-up as developed here, needs some improvements in monitoring the oxygen content. An exceptionally efficient way to speed up the process of corrosion degradation was the increase in temperature. However, the glass-reinforced plastic tank used for the test could become ductile at a temperature above 40°C. Thus, to speed up the corrosion process, a second circulation pump was mounted after approximately 210 days from the beginning of the test and a third circulation pump after 300 days. However, the introduction of the additional pump can also be seen as a mimic of the natural corrosion degradation when naturally or by forced cleaning, the corrosion layer is removed, and fresh oxygen is touching the metal surface, producing more accelerated corrosion degradation. In the current corrosion degradation test development, this was done at about 50% and 70 % of the total time duration of the corrosion testing. This phenomenon is also observed in real ship structures at about 10-12 years and 15-18 years of the service life of 25 to 30 years.

Considering the oxygen saturation at the beginning of testing, the estimated mean corrosion rate was 0.537 mm/year, which was very close to the experimentally observed value. After introducing a second circulation pump, the estimated corrosion rate increased to 0.57 mm/year and further with the third circulation pump up to 0.595 mm/year. However, the local flow of the water near the specimens was

even faster than the medium ones. The application of two additional circulation pumps led to a higher increase in corrosion degradation rates, as reported in Tables 2 and 5 for small-scale and large-scale specimens, respectively. The mean corrosion depth has been calculated as a fraction of initial plate thickness based on the percentage mass loss. Then, the corrosion rate has been estimated as a mean corrosion depth divided by the time needed for corrosion. The mass of small-scale specimens (Table 2) was determined using a laboratory scale with a precision of 0.1 g. In contrast, the mass of large-scale specimens (Table 5) was measured using the scale with an accuracy of 2 g.

## 4. Results and discussion

### *4.1. Analysis of corrosion degradation rate*

The most relevant statistical descriptors related to corrosion characteristics of small-scale specimens are presented in Table 2. The assumed target levels of corrosion degradation of the small-scale specimens were as follows: 3 %, 6 %, 8 %, 10 %, 12 %, 14 %, 16 %, 18 %, 20 % and 21 %. When the specimen reached its target degree of degradation level, it has been removed from the tank. Thus, not all specimens could be corroded along with the full duration of the tests. To monitor the current corrosion rate of the specimens, periodical mass measurements were carried out. For improved accuracy of the mass measurements, the specimens were cleaned each time there were measured. The reduction of specimen's thickness has been estimated based on the percentage reduction of specimen's mass. As can be noticed, the corrosion rates of 5 mm and 6 mm specimens were subjected to relatively low scatter.

In contrast, the corrosion rates of 8 mm specimens were subjected to a significantly higher spread. The mean corrosion rates of 6 mm specimens and 8 mm specimens were higher than the mean corrosion rate of 5 mm specimens. It can be noticed that the final degradation levels are slightly different from the assumed target levels, and there are originated from the mass deviation being a result of specimens chemical cleaning, which is discussed further.

**Table 2.** Corrosion statistics of small-scale specimens.

| No | Mass [g] | | Final DoD [%] | Elapsed days | Number of measurements [-] | Mean corrosion depth [mm] | Corrosion rate [mm/year] | | |
|---|---|---|---|---|---|---|---|---|---|
| | Initial | Final | | | | | Specimen | Mean | St. Dev. |
| 5.1 | 502 | 471 | 6.3 | 253 | 12 | 0.313 | 0.452 | 0.649 | 0.224 |
| 5.2 | 506 | 467 | 7.8 | 319 | 19 | 0.388 | 0.444 | | |
| 5.3 | 510 | 408 | 20.1 | 368 | 28 | 1.004 | 0.996 | | |
| 5.4 | 510 | 403 | 20.9 | 396 | 27 | 1.046 | 0.964 | | |
| 5.5 | 510 | 492 | 3.5 | 180 | 4 | 0.175 | 0.355 | | |
| 5.6 | 508 | 428 | 15.7 | 386 | 22 | 0.787 | 0.745 | | |
| 5.7 | 506 | 455 | 10.2 | 328 | 13 | 0.508 | 0.565 | | |
| 5.8 | 510 | 441 | 13.5 | 393 | 25 | 0.673 | 0.625 | | |
| 5.9 | 508 | 417 | 17.9 | 396 | 29 | 0.893 | 0.824 | | |
| 5.10 | 510 | 452 | 11.3 | 396 | 34 | 0.567 | 0.522 | | |
| 6.1 | 622 | 571 | 8.2 | 267 | 15 | 0.494 | 0.675 | 1.009 | 0.288 |
| 6.2 | 628 | 560 | 10.8 | 267 | 11 | 0.649 | 0.887 | | |
| 6.3 | 620 | 528 | 14.8 | 267 | 9 | 0.891 | 1.218 | | |
| 6.4 | 624 | 525 | 15.9 | 286 | 15 | 0.953 | 1.216 | | |

| | | | | | | | | | |
|---|---|---|---|---|---|---|---|---|---|
| 6.5 | 632 | 521 | 17.6 | 319 | 23 | 1.054 | 1.206 | | |
| 6.6 | 624 | 502 | 19.5 | 362 | 23 | 1.170 | 1.180 | | |
| 6.7 | 622 | 495 | 20.4 | 320 | 17 | 1.226 | 1.398 | | |
| 6.8 | 620 | 539 | 13.1 | 267 | 10 | 0.786 | 1.074 | | |
| 6.9 | 622 | 602 | 3.2 | 117 | 2 | 0.192 | 0.598 | | |
| 6.10 | 622 | 581 | 6.6 | 229 | 11 | 0.398 | 0.635 | | |
| 8.1 | 814 | 643 | 21.0 | 372 | 23 | 1.679 | 1.647 | | |
| 8.2 | 808 | 648 | 19.8 | 362 | 21 | 1.584 | 1.597 | | |
| 8.3 | 820 | 673 | 17.9 | 372 | 21 | 1.430 | 1.403 | | |
| 8.4 | 822 | 691 | 15.9 | 372 | 21 | 1.271 | 1.247 | | |
| 8.5 | 820 | 706 | 13.9 | 377 | 19 | 1.108 | 1.073 | 1.025 | 0.448 |
| 8.6 | 810 | 713 | 12.0 | 377 | 27 | 0.959 | 0.928 | | |
| 8.7 | 820 | 754 | 8.0 | 356 | 18 | 0.639 | 0.655 | | |
| 8.8 | 808 | 722 | 10.6 | 372 | 19 | 0.847 | 0.832 | | |
| 8.9 | 820 | 773 | 5.7 | 328 | 22 | 0.455 | 0.506 | | |
| 8.10 | 824 | 799 | 3.0 | 243 | 16 | 0.238 | 0.357 | | |

The corrosion degradation propagation in natural conditions could be estimated based on the non-linear time-dependent model of Guedes Soares and Garbatov (1998), defined as a function of time:

$$d(t) = \begin{cases} d_\infty \left[1 - \exp\left(-\dfrac{t-\tau_c}{\tau_t}\right)\right], & t > \tau_c \\ 0, & t \le \tau_c \end{cases} \quad (1)$$

where $d_\infty$ is the long-term corrosion depth, $\tau_c$ is the coating life and $\tau_t$ is the transition time.

However, when the governing factors (flow velocity, oxygen content) change or specimens are cleaned for measurements during testing from the corrosion products, the corrosion rate gets a new trend. In that case, the multi-trend model will be more suitable (Garbatov and Guedes Soares, 2007), which can be described as:

$$d(t) = \begin{cases} d_1(t) = d_{\infty,1}\left[1 - exp\left(-\dfrac{\left(t-\tau_{c,1}\right)}{\tau_{t,1}}\right)\right], & t_0 \le t \le t_1 \\ d_2(t) = d_1(t) + d_{\infty,2}\left[1 - exp\left(-\dfrac{\left(t-\tau_{c,2}\right)}{\tau_{t,2}}\right)\right], & t_1 \le t \le t_2 \\ \cdots & \\ d_n(t) = d_{n-1}(t) + d_{\infty,n}\left[1 - exp\left(-\dfrac{\left(t-\tau_{c,n}\right)}{\tau_{t,n}}\right)\right], & t_{n-1} \le t \le t_n \end{cases} \quad (2)$$

where n is the number of stages where the corrosion trend is changed.

Due to the application of additional circulation pumps, the three-stage corrosion model fits the experimental data. The first stage is between 0 and 210 days, the second stage is between 210 and 300 days, and the final stage is after 300 days. The coating life is considered equal to 0 for each stage. The transition time has decreased with any following stages and can be treated as a constant inside each stage. This is understandable since the surface will be already corroded, increasing the total area in contact with the new fresh air. The long-term corrosion depth has been found different for each stage

and individual specimen. The parameters found to fit the regressions with experimental data are presented in Table 3, including the range of the long-term corrosion depth regarding the thickness.

**Table 3.** Parameters of the fitted regression relationships for small-scale specimens.

| Specimen's thickness [mm] | Stage 1 | | Stage 2 | | Stage 3 | |
|---|---|---|---|---|---|---|
| | $\tau_t$ [days] | Range of $d_\infty$ [mm] | $\tau_t$ [days] | Range of $d_\infty$ [mm] | $\tau_t$ [days] | Range of $d_\infty$ [mm] |
| 5 | 300 | 0.22 ÷ 0.53 | 200 | 0.24 ÷ 0.50 | 150 | 0.05 ÷ 1.00 |
| 6 | 300 | 0.35 ÷ 1.37 | 200 | 0.30 ÷ 1.00 | - | - |
| 8 | 300 | 0.28 ÷ 1.27 | 200 | 0.00 ÷ 0.46 | 150 | 0.13 ÷ 1.10 |

In Figure 2, the corrosion depth versus time for all 5 mm specimens is presented. Notably, the progress of corrosion depth was evident, where at the beginning, the corrosion rate was lower than at the end of the corrosion process. Some points at the beginning of corrosion testing are observed slightly away from the regression curve. There is a visible period of approximately 50 days without corrosion degradation for some specimens, although no coating has been applied. This may be related to the initial thin layer of the black iron oxide, which comes from the rolling process and could act as initial protection from corrosion. Before corrosion testing, neither small-scale nor large-scale specimens were cleaned. This could be eventually considered as a separate stage in the multi-regression relationship. Finally, it is visible from Fig. 2 that the spread of the corrosion depth has been relatively low at a significant part of the corrosion degradation process. However, after introducing additional circulation pumps, the deviation increased significantly with time.

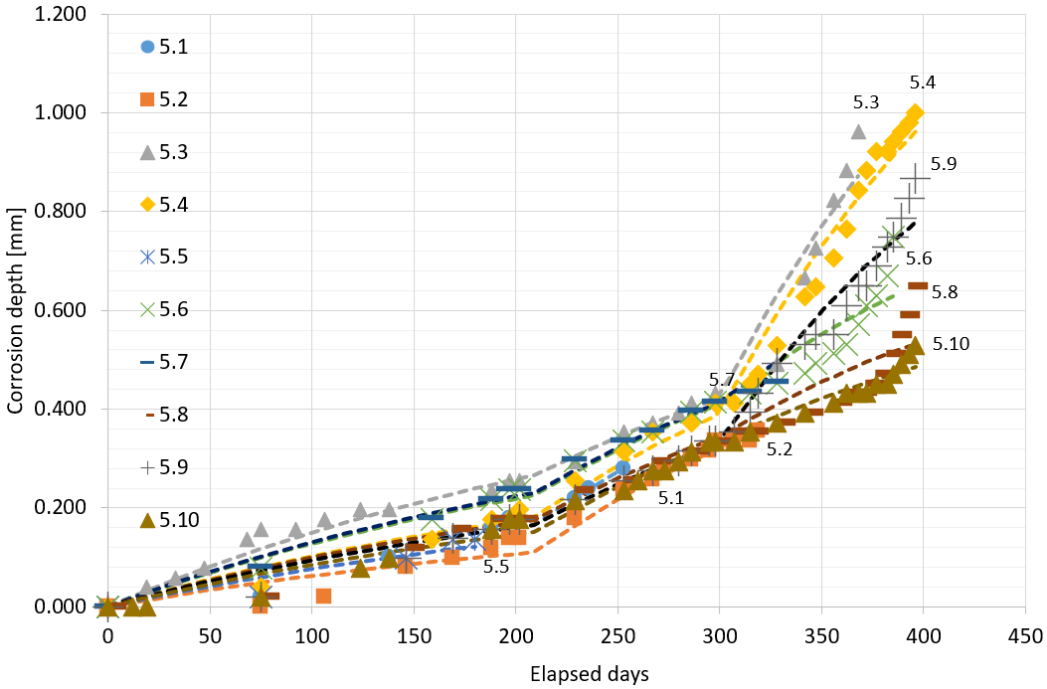


**Figure 2.** Corrosion depth of 5 mm specimens vs time.

The corrosion depth for 6 mm specimens is presented in Figure 3. In this case, two-stage regressions were also fitted since the corrosion was finished for almost all specimens before installing the third circulation pump. Similarly, to 5 mm specimens, the corrosion rate increased with the second stage. There was a significant deviation of the corrosion depth from the beginning of the corrosion process, which increased with time.

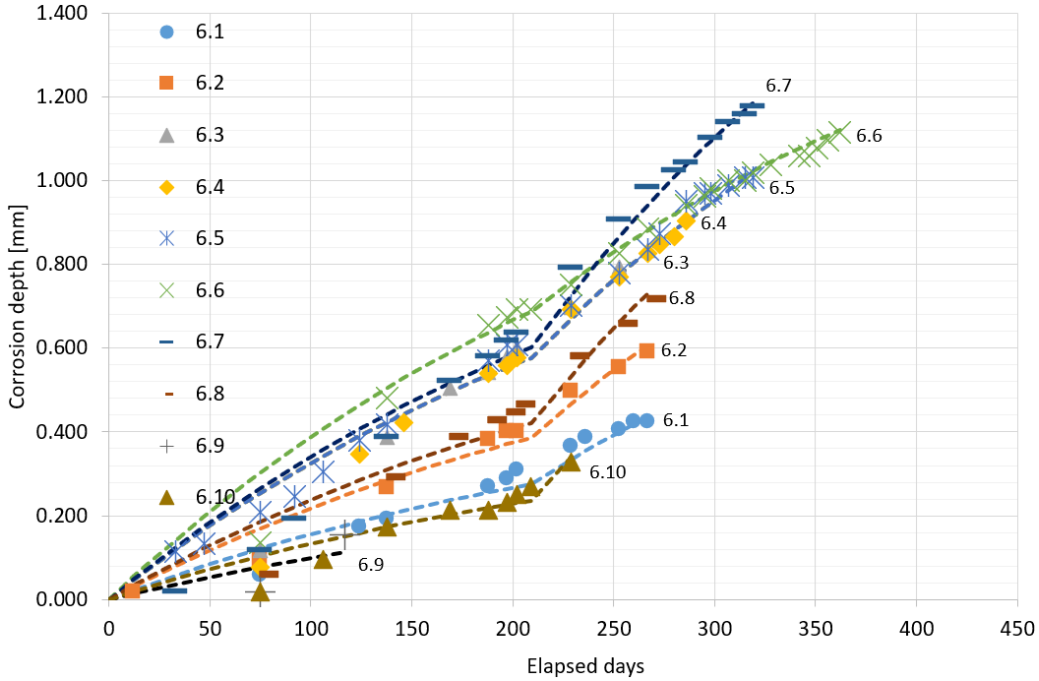


**Figure 3.** Corrosion depth of 6 mm specimens vs time.

The relation between the corrosion depths of 8 mm specimens and testing time has been presented in Figure 4. In this case, the corrosion has been active from the beginning of the process. The three-stage regression has also been applied. A significant increment of the corrosion rate for many specimens was observed after introducing the third circulation pump. The corrosion rate has also been significantly scattered, which increased with the corrosion degradation development. As a result, the standard deviation is considerably higher for the 8 mm specimens than for both 5 mm and 6 mm specimens (see Table 2).

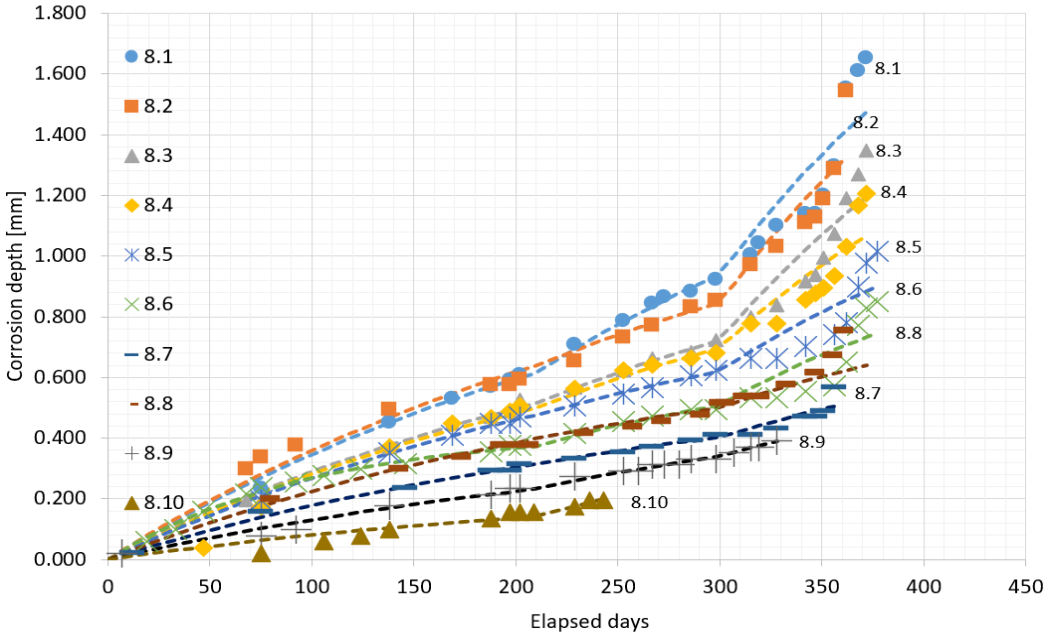


**Figure 4.** Corrosion depth of 8 mm specimens vs time.

To find one equation that could describe the corrosion process, the one long-term corrosion depth that could model the mean corrosion depth propagation has been found for each stage and the initial thickness of the specimens. As can be noticed, the values describing any individual specimen presented in Table 3 may deviate from the ones shown as a mean value in Table 4. Thus, the couple specimens of

each thickness need to be provided to account for that uncertainty. The significant scatter is also observed in Figures 2 – 4.

**Table 4.** Parameters of the fitted regression relationships for small-scale specimens (one regression in each thickness).

| Specimen's thickness [mm] | Stage 1 | | Stage 2 | | Stage 3 | |
|---|---|---|---|---|---|---|
| | $\tau_t$ [days] | Range of $d_\infty$ [mm] | $\tau_t$ [days] | Range of $d_\infty$ [mm] | $\tau_t$ [days] | Range of $d_\infty$ [mm] |
| 5 | 300 | 0.37 | 200 | 0.33 | 150 | 0.53 |
| 6 | 300 | 0.92 | 200 | 1.00 | - | - |
| 8 | 300 | 0.83 | 200 | 0.30 | 150 | 0.66 |

The corrosion statistical descriptors for large-scale specimens are presented in Table 5, and the target levels of degree of degradation were as follows: 7 %, 14 % and 21 %. It could be noticed that the mean corrosion rate of 5 mm and 6 mm specimens is very close to the initially predicted one. In 8 mm specimens, the mean corrosion rate was higher than the initially assessed one. It may be concluded that due to the use of two additional circulation pumps, the observed mean corrosion rate was close to the initially estimated one. However, the oxygen content has been lower than assumed initially (see Section 2). The corrosion testing tends to produce severe corrosion degradation in an accelerated manner. The target level of the maximum corrosion degradation level was assumed to be 21%. Three different degradation levels were assumed for each plate thickness, *i.e.*, 7%, 14 % and 21 %. During structural inspections, the elements with the mean corrosion depth of approx. 20 % - 25 % are typically replaced. Seven measuring periods have been planned for the most severely corroded specimens in (Woloszyk and Garbatov, 2021). Due to the cleaning of specimens from corrosion products and the specified prior mass measurements.

Nevertheless, the deviation did not exceed the 0.5 % of degradation level. Finally, it could be noticed that the corrosion rates deviate between specimens. A similar level of approximately 30% of COV is observed for 5 mm and 6 mm specimens. However, the deviation in the case of 8 mm specimens reaches a significant level of 50%.

**Table 5.** Parameters of the fitted regression relationships for small-scale specimens.

| Thickness [mm] | No | Mass [kg] | | Final DoD [%] | Corr. depth [mm] | Elapsed days | Number of measurements [-] | Corrosion rate [mm/year] | | |
|---|---|---|---|---|---|---|---|---|---|---|
| | | Initial | Final | | | | | Specimen | Mean | St. Dev. |
| 5 | 1.5 | 25.07 | 23.25 | 7.24 | 0.362 | 264 | 3 | 0.501 | 0.774 | 0.266 |
| | 2.5 | 25.04 | 19.77 | 21.05 | 1.053 | 372 | 7 | 1.033 | | |
| | 4.5 | 25.00 | 21.60 | 13.60 | 0.680 | 315 | 5 | 0.788 | | |
| 6 | 1.6 | 30.77 | 26.63 | 13.46 | 0.808 | 382 | 7 | 0.772 | 0.745 | 0.311 |
| | 3.6 | 30.72 | 24.46 | 20.37 | 1.222 | 428 | 12 | 1.042 | | |
| | 4.6 | 30.79 | 28.74 | 6.67 | 0.400 | 347 | 7 | 0.421 | | |
| 8 | 1.8 | 40.43 | 34.86 | 13.80 | 1.104 | 382 | 7 | 1.055 | 1.146 | 0.521 |
| | 2.8 | 40.48 | 37.72 | 6.84 | 0.547 | 295 | 4 | 0.677 | | |
| | 3.8 | 40.55 | 31.49 | 22.34 | 1.787 | 382 | 7 | 1.707 | | |

To investigate the corrosion degradation progress, the three-stage regressions have been plotted similarly to small-scale specimens. The propagation of corrosion degradation with time for all large-scale specimens is presented in Figure 5. The transition times in each stage were the same as in the case of small-scale specimens (see Table 3). Similarly to small-scale specimens, the corrosion rate increased with the following stages. There has been significant scatter for 8 mm specimens, where the corrosion processes of 1.8 and 2.8 specimens were similar, and the 3.8 specimens occurred to corrode almost two times faster. In other thicknesses, the differences between specimens in terms of corrosion rate were not that radical.

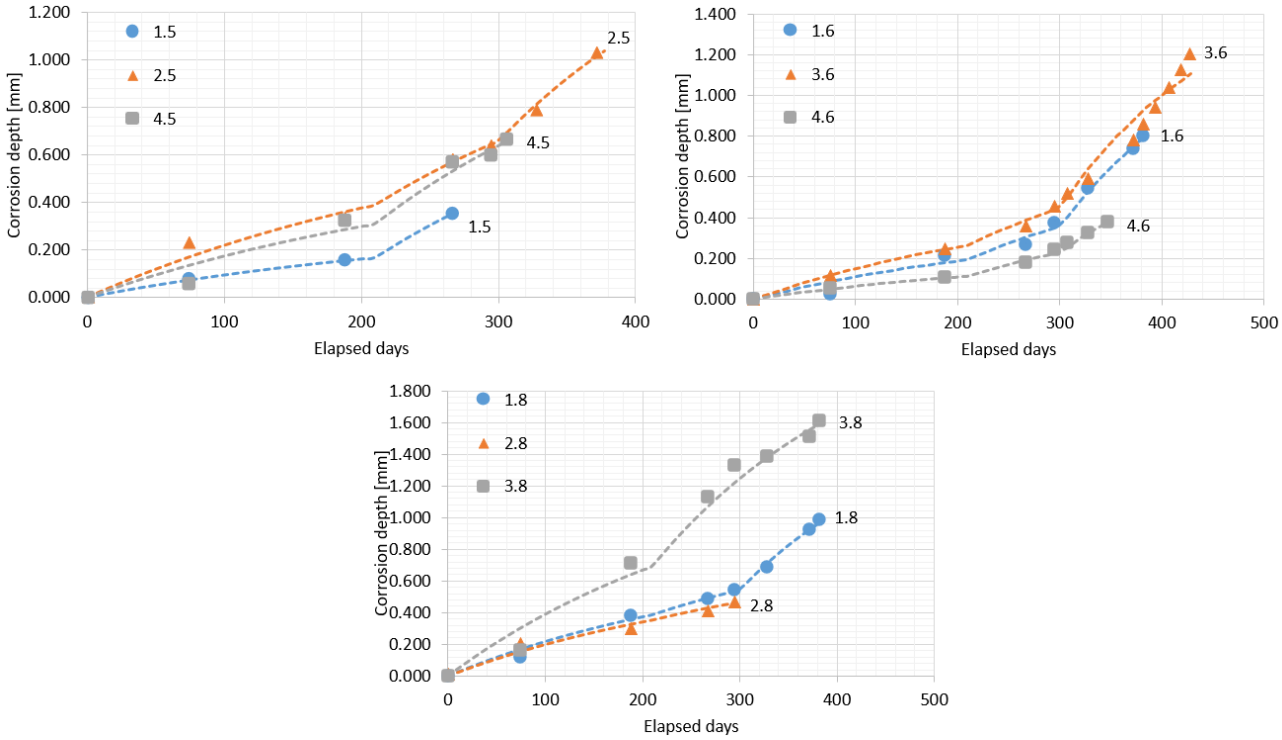


**Figure 5.** Corrosion diminutions of large-scale specimens vs time for 5 mm (left – top), 6 mm (right-top) and 8 mm (bottom) specimens.

The corrosion degradation developed during the experimental test is compared with the real measurement of deck plates of ballast and cargo tanks as given by ABS (ABS, 2002; Wang et al., 2003) and analysed by Garbatov et al. (2006). The data provided by ABS covered 1168 real corrosion measurements for ballast and 4665 for cargo tank plates on ships with a length in the range of 163 to 401 mm and age from 12 to 32 years. The frequency scatter diagram of corrosion depts as a function of time is shown in Fig. 6. It can be noticed that there is a very high scatter of the measured corrosion depths, similarly to in the current experiment. The measured corrosion depths during the experiment (Figure 7) are compared with the real in-situ measurements in deck plates in ballast and cargo tanks (Figure 6), represented by their mean value represented by solid curves. The mean value of corrosion depths for deck panels is compared with the experimental results obtained for the small-scale and large-scale specimens. Compared to the results, the time from the accelerated tests is scaled by a time factor, defined as the lowest mean square error between the reported mean value of the measurements analysed in (Garbatov et al., 2006) and the current experiment. The coating life is added to the time in the accelerated tests since the specimens were not coating protected. The resulting acceleration factor is estimated as 4.3, 9.6 and 7.4 for 5 mm, 6 mm, and 8 mm for the small-scale specimens and 7.0, 6.0, and 10.7 for 5 mm, 6 mm, and 8 mm stiffened plates, respectively. As shown in Figure 7, these results are consistent with the mean corrosion rates reported in Table 6. Similar corrosion depths were achieved after 400 days of accelerated corrosion testing, like many years of natural corrosion as the corrosion depths analysed in (Garbatov et al., 2006). The trend of degradation also looks very similar. This comparison also confirms that the developed experimental set-up and the approach used to

control the progress of corrosion degradation are efficient, reliable, and can reproduce the real, in situ corrosion degradation of marine structures, which can be used in the structural integrity analysis of the structural integrity analysis ageing structures.

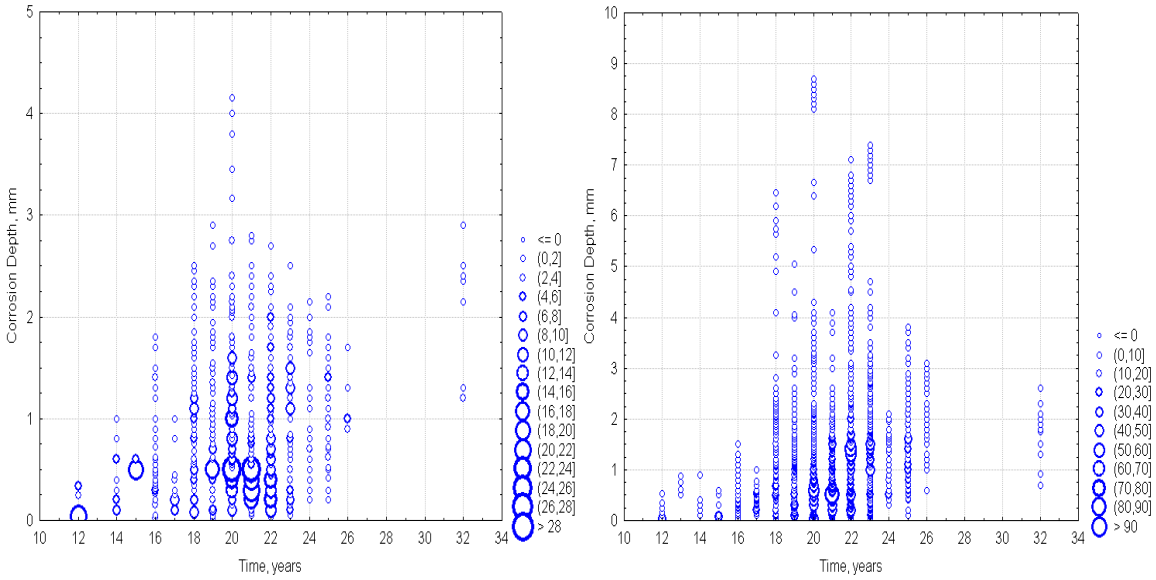


**Figure 6.** Frequency scatter diagram of corrosion depth of deck plates of ballast (left) and cargo (right) tanks (Garbatov et al., 2006).

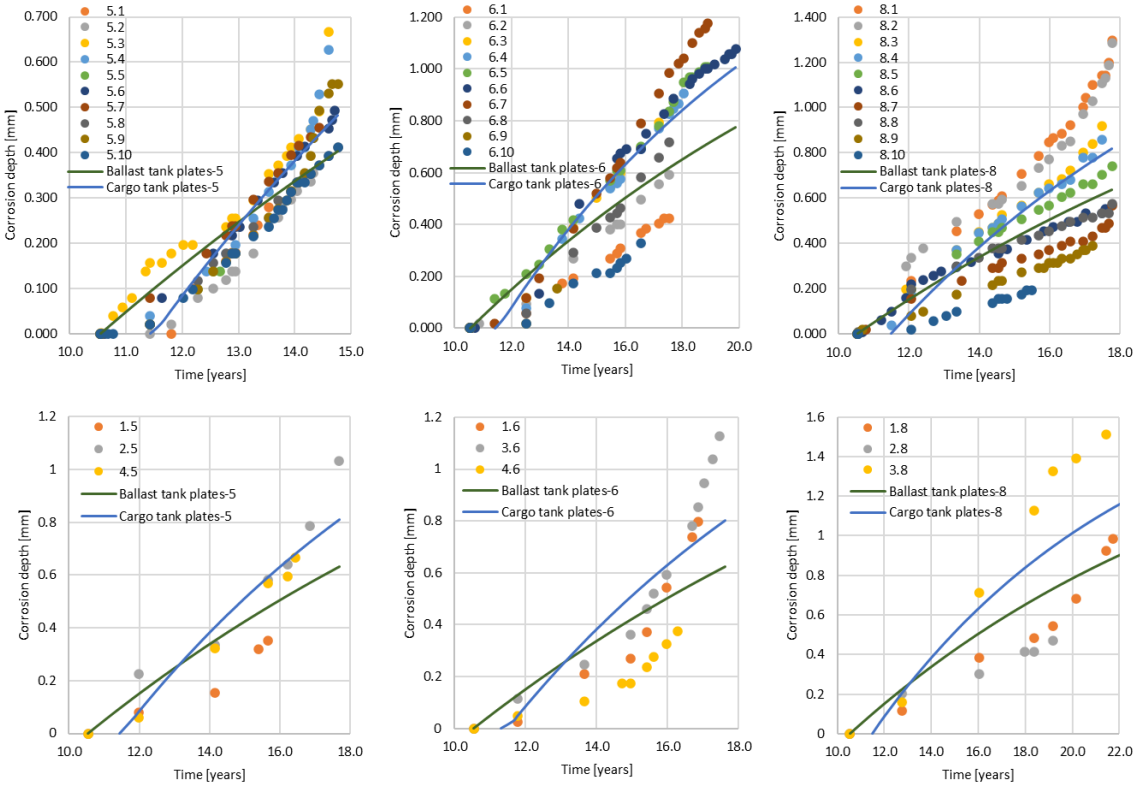


**Figure 7.** Corrosion depth as a function of time of specimens and deck plates of ballast and cargo tanks (Garbatov et al., 2006) compared to small-scale specimens - 5 mm (left-top), 6 mm (mid-top), 8 mm (right-top) and stiffened plates - 5 mm (left-bottom), 6 mm (mid-bottom), 8 mm (right-bottom).

*4.2. Corrosion degradation correlation*

The primary reason to corrode the small-scale coupons was to investigate the changes in mechanical properties. However, this type of specimen is commonly used to estimate the corrosion rate of large-scale specimens. The mass measurements of such elements are more accessible and faster. Thus, in the presented section, the correlation between corrosion rate and corrosion trends between large-scale and small-scale specimens is discussed, and the feasibility of this methodology is analysed.

The comparison between the corrosion rates of large-scale and small-scale specimens is presented in Table 6. It could be noticed that the mean corrosion rates of small-scale and large-scale specimens are different. The highest deviation is observed for 6 mm specimens where corrosion of coupons was almost 50% faster than stiffened plates. In both 5 mm and 8 mm thicknesses, the mean values of the corrosion rate of large-scale specimens were higher by 19% and 12%, respectively. Therefore, it could be considered as somewhat similar values. The Coefficient of Variation is relatively equal for both scales. Thus, the lowest is observed for 5 mm and 6 mm specimens and the highest for 8 mm specimens. It is noted that corrosion rates and standard deviations are generally higher for 8 mm specimens than 5 mm and 6 mm specimens. One possible reason could be different surface roughness in the delivery state, impacting corrosion rate (Toloei et al., 2013). Although the same material was for all plates, the batches of steel could vary in the delivery state.

**Table 6.** Comparison between corrosion rate in small-scale and large-scale specimens.

| Thickness [mm] | Corrosion rate [mm/year] | | | | | |
|---|---|---|---|---|---|---|
| | Large-scale specimens | | | Small-scale specimens | | |
| | Mean | St. Dev. | COV [%] | Mean | St. Dev. | COV [%] |
| 5 | 0.774 | 0.266 | 34.4 | 0.649 | 0.224 | 34.4 |
| 6 | 0.745 | 0.311 | 41.8 | 1.009 | 0.288 | 28.5 |
| 8 | 1.146 | 0.521 | 45.5 | 1.025 | 0.448 | 43.7 |

Estimating the corrosion rate of large-scale specimens based on the corrosion of coupons has limited reliability, especially when considering 6 mm plates. One possible reason could be the non-homogeneity of the physical factors of the water in the tank. Although the temperature and salinity are somewhat constant, the water circulation and oxygen saturation could variate through the tank. One can notice that with the installation of two additional circulation pumps, the increase of corrosion rate was observed for almost all stiffened plates. Due to their large scale, there is no sensitivity to local variations of factors (oxygen content, flow velocity and temperature). However, in small-scale specimens, an increment of the corrosion rate was not captured for all of them. It is impossible to provide constant water velocity and oxygen saturation in the tank due to the localised water sources inlet and the pipe, where air bubbles are created. In the case of in-situ measurements, the conditions will be more homogenous, and the correlation between the corrosion rate of large-scale and small-scale specimens. Nevertheless, the deviations will be noted too.

A general conclusion is that corrosion testing in laboratory conditions, where the tank is of limited dimensions, the corrosion rate of small specimens will not match the estimated corrosion rate of plates of a larger scale. Eventually, some re-designing of the set-up could provide more homogenous conditions concerning oxygen saturation and water velocity.

*4.3. Surface characteristics of corroded small-scale specimens*

Corrosion products need to be removed to analyse the surfaces of corroded specimens. Thus, cleaning with the use of a chemical solution has been applied (see Figure 8). The cleaning was performed using water, hydrochloric acid, which dissolved the corrosion products and corrosion inhibitor, preventing dissolution of steel by acid. To avoid further atmospheric corrosion, the specimens were cleaned and dried. The final mass of the specimen has been measured after the corrosion process, revealing that the corrosion products could disturb the measurement of the degradation level up to 1.5 %.

(**a**) (**b**)

**Figure 8.** The example of specimen: (a) before cleaning; (b) after cleaning.

Further, after the cleaning process, the detailed microscopic measurements of corroded surfaces have been carried out using the microscope Keyence VHX-7000.

The detailed 3D reproduction of the corroded surfaces has been obtained with the mesh size of 2 μm x 2 μm. An example of such a scanned corroded surface could be seen in Figure 9. It is noted that only the gauge length of the specimen has been scanned because this part is relevant during tensile testing, whereas mounting parts are not important. Additionally, the range of the possible area that could be captured via a microscope has been limited.

**Figure 9.** An example of a scan of the corroded surface (specimen 6.3).

The scans of corroded surfaces were further analysed, and the sample thickness map of corroded specimens is presented in Figure 10, where both top and bottom surfaces are shown.

It could be noticed that the specimens immersed in water develop different corrosion fields when compared to other corrosion types, such as atmospheric corrosion (Wang and Moan, 1996). In this experiment, the regions of either low or significant corrosion diminutions are relatively widespread, purely demonstrating that no pitting corrosion is observed. However, even in such small specimens, the observed variances show that the general corrosion degradation is also non-uniform. Nevertheless, by following different specimens, one cannot establish a typical pattern, implying that nature is fully stochastic.

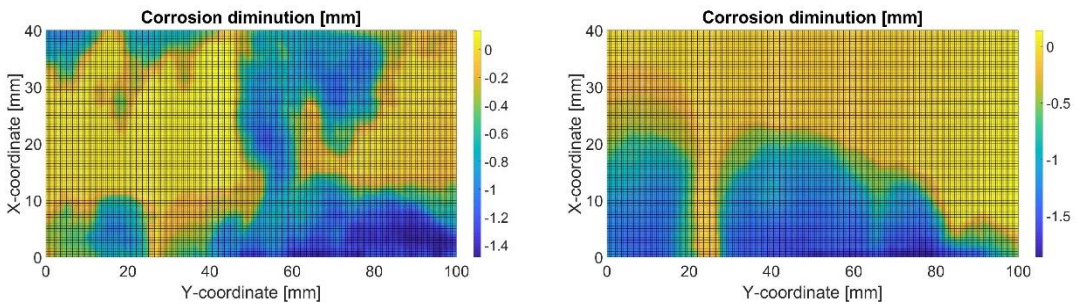


(**a**) (**b**)

**Figure 10.** Corrosion diminutions of specimen 6.3: (a) top surface; (b) bottom surface.

The corrosion surface's statistical descriptors are obtained based on the information gathered from the scanning of the specimens, as presented in Table 7. The specimens are sorted with the ascending order of Degree of Degradation. It needs to be noted here that the DoDs reported there could be different from those presented in Table 2. In Table 2, the total mass loss of the entire specimen is used for DoD calculation. However, for strength analysis, only corrosion characteristics of the specimen without mounting parts are relevant. Thus, the calculated DoD, presented in Table 7, was based on the obtained corrosion characteristics from the 3D scans. Nevertheless, in most cases, the differences in calculated DoDs are not exceeding 2%. Further, the following statistics are presented: maximum residual thickness ($t_{max}$), maximum corrosion depth of upper surface ($d_{u,max}$), mean corrosion depth of upper surface ($d_{u,mean}$), a standard deviation of corrosion depth of upper surface ($d_{u,StDev}$), similar statistics related to the bottom surface ($d_{b,max}$, $d_{b,mean}$, $d_{b,StDev}$), minimum residual thickness ($t_{min}$) and minimum cross-sectional area ($A_{min}$).

**Table 7.** Statistical descriptors of the small-scale specimens.

| No | $DoD$ [%] | $t_{max}$ [mm] | $d_{u,max}$ [mm] | $d_{u,mean}$ [mm] | $d_{u,StDev}$ [mm] | $d_{b,max}$ [mm] | $d_{b,mean}$ [mm] | $d_{b,StDev}$ [mm] | $t_{min}$ [mm] | $A_{min}$ [mm²] |
|---|---|---|---|---|---|---|---|---|---|---|
| 5.5 | 3.2 | 5.00 | 0.741 | 0.087 | 0.177 | 0.587 | 0.072 | 0.085 | 3.82 | 191.5 |
| 5.6 | 5.9 | 5.00 | 1.597 | 0.207 | 0.184 | 1.038 | 0.089 | 0.211 | 3.11 | 180.9 |
| 5.2 | 7.4 | 4.98 | 1.530 | 0.321 | 0.516 | 0.345 | 0.051 | 0.047 | 3.21 | 174.3 |
| 5.1 | 8.0 | 5.00 | 1.264 | 0.230 | 0.342 | 0.664 | 0.170 | 0.117 | 3.24 | 179.0 |
| 5.7 | 13.1 | 4.94 | 1.629 | 0.170 | 0.358 | 1.857 | 0.484 | 0.540 | 1.76 | 157.6 |
| 5.9 | 15.4 | 5.00 | 2.508 | 0.538 | 0.839 | 1.233 | 0.231 | 0.242 | 1.40 | 156.9 |
| 5.8 | 15.4 | 5.00 | 2.269 | 0.588 | 0.814 | 0.798 | 0.182 | 0.103 | 2.39 | 162.4 |
| 5.4 | 15.5 | 5.00 | 2.017 | 0.444 | 0.622 | 0.983 | 0.331 | 0.231 | 2.26 | 147.8 |
| 5.10 | 16.0 | 4.99 | 1.996 | 0.757 | 0.730 | 0.470 | 0.042 | 0.033 | 2.92 | 164.2 |
| 5.3 | 24.3 | 5.00 | 2.016 | 0.884 | 0.680 | 1.661 | 0.332 | 0.308 | 2.20 | 116.6 |
| 6.9 | 2.2 | 6.00 | 0.46 | 0.047 | 0.106 | 0.423 | 0.084 | 0.068 | 5.22 | 231.1 |
| 6.10 | 6.3 | 6.00 | 1.04 | 0.302 | 0.294 | 0.339 | 0.078 | 0.080 | 4.64 | 214.1 |
| 6.1 | 6.8 | 6.00 | 1.32 | 0.338 | 0.376 | 0.176 | 0.069 | 0.018 | 4.75 | 211.5 |
| 6.2 | 9.6 | 6.00 | 1.49 | 0.555 | 0.509 | 0.262 | 0.018 | 0.038 | 4.38 | 189.6 |
| 6.4 | 12.3 | 6.00 | 1.46 | 0.630 | 0.421 | 1.302 | 0.107 | 0.303 | 3.42 | 183.6 |
| 6.3 | 14.1 | 6.00 | 1.61 | 0.397 | 0.438 | 1.900 | 0.447 | 0.529 | 2.69 | 178.6 |
| 6.8 | 14.7 | 6.00 | 1.70 | 0.517 | 0.421 | 1.864 | 0.366 | 0.380 | 2.66 | 187.6 |
| 6.5 | 16.6 | 6.00 | 0.75 | 0.018 | 0.060 | 1.938 | 0.975 | 0.595 | 4.06 | 172.4 |
| 6.6 | 17.6 | 6.00 | 2.21 | 1.025 | 0.606 | 0.938 | 0.029 | 0.101 | 3.33 | 177.6 |
| 6.7 | 21.3 | 5.95 | 2.17 | 0.333 | 0.330 | 2.032 | 0.947 | 0.385 | 2.31 | 174.4 |
| 8.10 | 1.7 | 8.00 | 0.602 | 0.083 | 0.191 | 0.288 | 0.051 | 0.079 | 7.26 | 300.8 |
| 8.9 | 4.0 | 8.00 | 0.262 | 0.060 | 0.045 | 0.940 | 0.262 | 0.237 | 6.93 | 287.6 |
| 8.4 | 12.3 | 8.00 | 2.713 | 0.774 | 0.691 | 3.080 | 0.208 | 0.359 | 2.51 | 234.3 |
| 8.6 | 13.8 | 7.86 | 1.498 | 0.275 | 0.240 | 1.966 | 0.827 | 0.598 | 4.99 | 239.8 |

| | | | | | | | | | | |
|---|---|---|---|---|---|---|---|---|---|---|
| 8.7 | 14.1 | 8.00 | 1.574 | 1.058 | 0.453 | 0.512 | 0.071 | 0.051 | 6.03 | 260.8 |
| 8.2 | 14.8 | 8.00 | 2.832 | 0.935 | 0.773 | 1.144 | 0.248 | 0.116 | 4.56 | 238.1 |
| 8.5 | 15.6 | 8.00 | 1.996 | 0.461 | 0.597 | 1.931 | 0.785 | 0.469 | 4.33 | 234.1 |
| 8.8 | 16.9 | 7.81 | 1.107 | 0.249 | 0.126 | 1.909 | 1.100 | 0.681 | 5.51 | 249.0 |
| 8.3 | 18.4 | 8.00 | 1.752 | 0.148 | 0.214 | 2.814 | 1.324 | 0.741 | 4.40 | 215.2 |
| 8.1 | 28.4 | 7.79 | 2.750 | 0.913 | 0.627 | 3.073 | 1.362 | 0.709 | 3.03 | 188.3 |

It could be noticed that with the increase of corrosion degradation, the maximum and mean values of the corrosion depth are increasing. The ratio between maximum and mean corrosion depth for all corrosion fields ranges between 1.49 up to 41.8, with the mean value equal to 6.29. This generally shows that locally specimens are much strongly corroded when compared to the mean corrosion diminution. There was no found correlation between this value and degradation level.

The standard deviation increases as well with the corrosion development. When analysing the ratio between standard deviation and the mean value of corrosion depth, which informs about the corrosion field's irregularity, the value deviates between 0.26 and 3.48. The mean value of this ratio is equal to 1.16. The lowest mean value was obtained for 8 mm specimens, which was below 1. These values were higher in both 5 mm and 6 mm specimens, showing that corrosion was more irregular for those specimens. No correlation between that ratio and corrosion degradation level was found.

Although both surfaces were equally subjected to the corrosion process, the mean corrosion depth is significantly higher for one of the surfaces in almost most cases. A few specimens were similarly corroded on both sides (5.1, 5.4, 5.5, 6.3). However, for most specimens, the mean corrosion depth of one side was approximately three times smaller than another side.

Interestingly, the maximum residual thickness was for the specimens with equal initial thickness for almost all specimens. Thus, although the corrosion was general, there were places untouched by the degradation process.

It is noted that both minimum cross-sectional area and minimum residual thickness are decreasing with the corrosion development. There are observed extreme values for some specimens regarding initial thickness in minimum thickness (5.7, 5.9, 6.3, 6.7, 6.8, 8.1, 8.4). The minimum thickness is below half of the initial thickness for those specimens, which shows substantial irregularity of the observed corrosion fields. In the case of minimum cross-sectional area, it is observed that for all specimens, that value is lower when compared to the cross-sectional area resulting from mean corrosion depth. For all specimens, the mean difference between the minimum cross-sectional area and one that resulted from uniform loss is equal to 10.5 %, where 1.1 % and 29.8 % are extreme differences. It is noted that with the increase of the degradation level, this difference is increasing too. Additionally, there are observed higher differences with the rise of initial specimen thickness.

*4.4. Surface characteristics of corroded large-scale specimens*

In the case of large-scale specimens, the general thickness distribution has been captured via ultrasonic measurements. The corrosion products have been removed manually to avoid the destruction of corroded surfaces. After some time of the specimens drying, the corrosion products started to detach from the surface. Only additional manual removing was sufficient to provide a clear surface and perform the ultrasonic measurements. The final mass was captured without corrosion products. The degradation level was up to 2% smaller compared to non-cleaned specimens – some examples of corroded stiffened plates were presented in Figure 11.

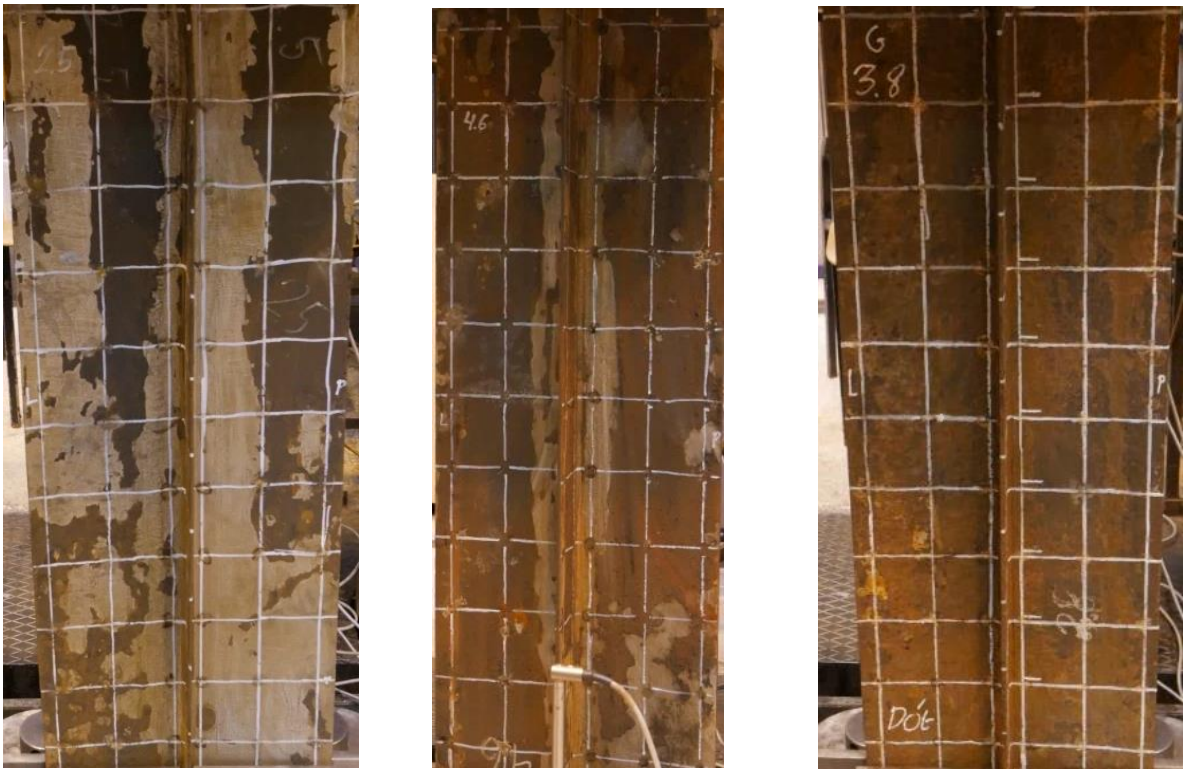


(**a**) (**b**) (**c**)

**Figure 11.** Corroded stiffened plates examples: (a) 2.5; (b) 4.6; (c) 3.8.

Using the statistical descriptors of the targeted trend of the corrosion depth as a function of time and assuming that at any instant of time it follows the Normal distribution, the $n$ number of measurements conditional to the confidence level and margin of error can be estimated as this suggested by Dowdy et al. (2004) and used in the corrosion set-up as presented in (Woloszyk and Garbatov, 2021) within the following margin:

$$\bar{d}(t) - \frac{u_\alpha \sigma(t)}{\sqrt{n}} \leq m \leq \bar{d}(t) + \frac{u_\alpha \sigma(t)}{\sqrt{n}} \tag{3}$$

where $u_\alpha$ is the percentile of the N(0,1) distribution with the assumed confidence level $\alpha$, $\bar{d}(t)$ and $\sigma(t)$ are the mean value and standard deviation of corrosion depth, respectively. The standard error is defined as $(u_\alpha \sigma(t))/\sqrt{n}$ and when the increment of corrosion depth degradation, $\Delta d(t)$ is divided by the corrosion depth at the time t, $\bar{d}(t)$, the error is defined as $Err = \Delta d(t)/\bar{d}(t)$. To ensure the assumed standard error and confidence level, the required number of measurements is estimated as:

$$n = \left( \frac{u_\alpha \sigma(t)}{\text{Err}} \right)^2 \tag{4}$$

The relationship between the number of measurements and testing time is almost linear, but the number of measures as a function of standard error and confidence are non-linear. With the decrease of the standard error, the measuring effort significantly increases and in the case of the confidence level, the measuring effort increase for higher values. The measurement control, the number of measurements, and corrosion depth for the present corrosion testing set-up assume a confidence level of 95% and an error value of 10%.

Seventy-eight points in a plate and 24 points in the stiffener has been measured from both sides to measure the thickness distribution accurately. Thus, the 208 measurement points for each stiffened plate were captured, considering the regular distance between grid points. The applied grid can be observed in Figure 11. If the plate is ideally flat from both sides, the observations of the thickness

measured from each side will be identical. However, as presented in (Cegla and Gajdacsi, 2016), if the back wall surface is irregular (such as corroded one), the ultrasonic measurements could be distracted. Thus, in this study, the measurements were performed from both sides of the plate. In pre-experimental research (Woloszyk and Garbatov, 2021), the optimum number of measuring points has been estimated equal to 98 for the most severely corroded plate. However, even for not severely corroded plates, accurate information about thickness distribution and the possible application of thickness distribution into the numerical model is essential.

In Table 8, the statistics concerning the gathered information from ultrasonic measurements are presented. It was identified that local non-uniformity of the surface of the corroded specimen could lead to a significant overestimation of the thickness at a particular point. In general, the highest local irregularities were observed for 8 mm specimens. For most strongly corroded 3.8 specimen, this difference reaches the level of 0.5 mm, which is way above the acceptable error of ultrasonic equipment itself (0.1 mm). In the case of 5 mm specimens, relatively flat regions of the plate made possible accurate measurements. In that case, the differences between mass measurements and ultrasonic ones were within the acceptable error level. However, when one considers the thickness, calculated as the mean value from both sides of the plate, it is higher for all specimens when compared with accurate mass measurements. Therefore, the closest results are obtained for a minimum value of thickness from two sides of the plate, and those should be considered in further analysis. In this view, in real ships, the measurements are carried out usually only on one side of the plate; thus, significant overestimations could be obtained. Additionally, for in situ measurements, the lower number of thickness points is collected, which could be another source of uncertainty.

**Table 8.** Statistics of ultrasonic measurements.

| Specimen | Residual thickness [mm] | | | | |
|---|---|---|---|---|---|
| | Mean - mass | Mean – 1st side | Mean – 2nd side | Mean from 2 sides | Minimum from 2 sides |
| 1.5 | 4.638 | 4.735 | 4.682 | 4.709 | 4.633 |
| 2.5 | 3.948 | 4.051 | 4.121 | 4.086 | 3.891 |
| 4.5 | 4.320 | 4.410 | 4.318 | 4.364 | 4.248 |
| 1.6 | 5.192 | 5.428 | 5.355 | 5.391 | 5.220 |
| 3.6 | 4.778 | 5.081 | 5.034 | 5.057 | 4.894 |
| 4.6 | 5.600 | 5.865 | 5.753 | 5.809 | 5.668 |
| 1.8 | 6.896 | 7.301 | 7.312 | 7.306 | 7.135 |
| 2.8 | 7.453 | 7.557 | 7.633 | 7.595 | 7.522 |
| 3.8 | 6.213 | 6.719 | 6.691 | 6.705 | 6.501 |

The thickness distribution maps have been obtained based on the measurements, with the interpolated values between the grid's points. It is noted that the distribution is non-uniform for all specimens.

The distributions for stiffened plates of initial 5 mm thickness are presented in Figures 12 – 14. The distribution for a 1.5 mm stiffened plate, which corresponds to 7% of DoD, is shown in Figure 12. In this case, the higher corrosion diminutions are observed on the right side of the plate, and the lower thickness is in the bottom part of the stiffener. In Figure 13, the residual thickness for a 4.5 stiffened plate is presented. In general, the lowest thickness is observed near the stiffener in the welding zone, and the stiffener itself significantly deteriorates. The thickness distribution for a plate with a 21% degradation level (2.5) is presented in Figure 14. It is noted that, similarly to the previous specimen, high corrosion depths are observed near the welding zone of the specimen. Additionally, the right side

of the plate is strongly corroded in comparison to the left one. The stiffener itself is relatively uniformly corroded

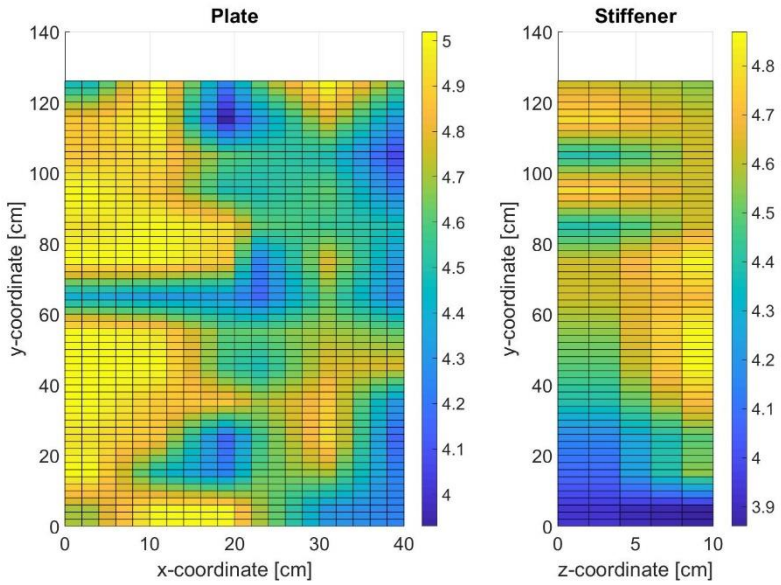


**Figure 12.** Thickness distribution in 1.5 specimen (7% of DoD) [mm].

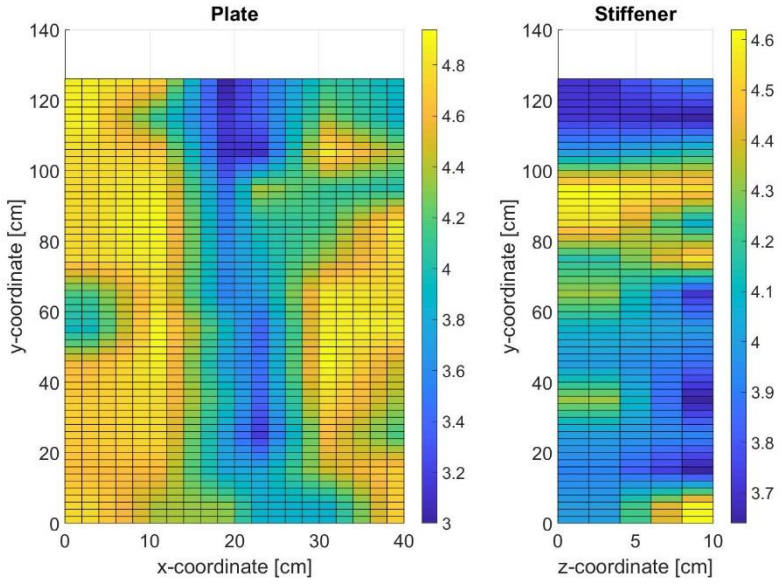


**Figure 13.** Thickness distribution in 4.5 specimen (14% of DoD) [mm].

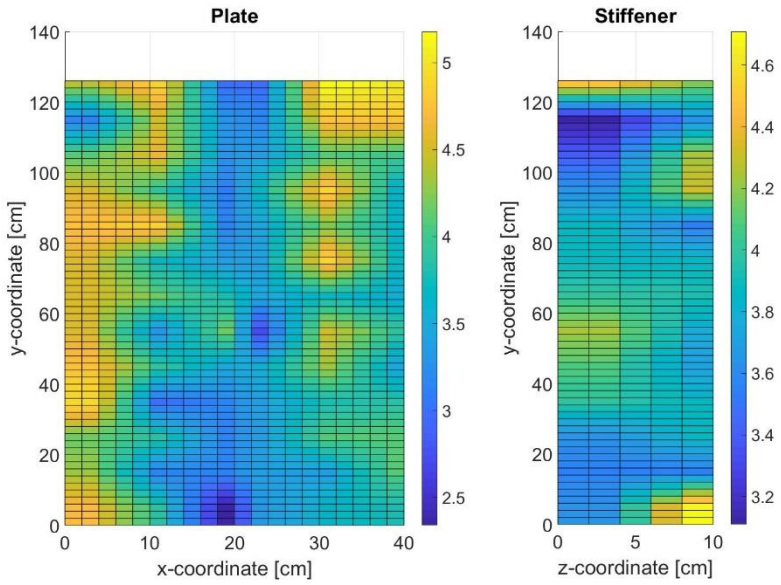


**Figure 14.** Thickness distribution in 2.5 specimen (21% of DoD) [mm].

The distributions for plates with an initial thickness of 6mm are presented in Figures 15 – 17. It is noted that the thickness distributions for plates with 7% and 14% of DoD (Figures 15 and 16, respectively) are similar. The highest corrosion diminutions are concentrated near the welding region and some places on the plate edges. In the case of stiffeners, in the 4.6 specimen (Figure 15), the middle part is rather non-corroded, opposite upper and lower regions. In specimen 1.6 (Figure 16), the stiffener is corroded primarily near the welding, and higher corrosion depths are observed near the free edge. In the 3.6 specimen (see Figure 17), extensive corrosion for both plate and stiffener is kept near the specimen's welding zone and upper part.

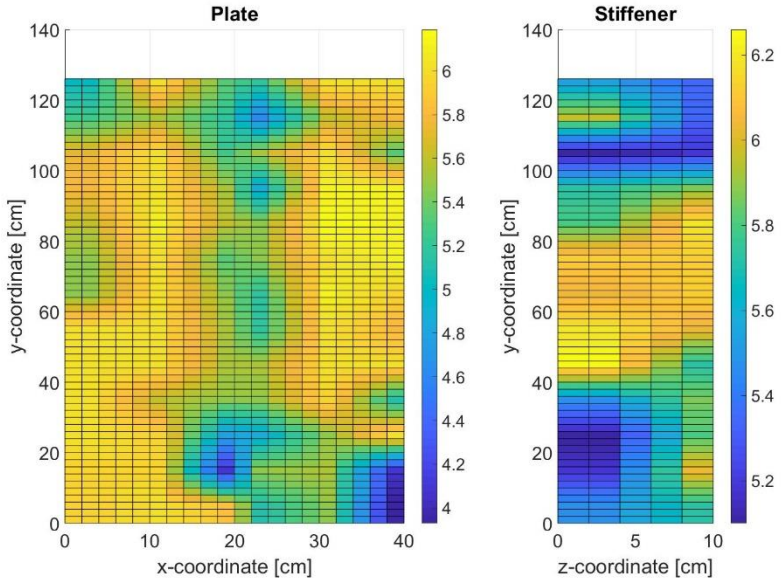


**Figure 15.** Thickness distribution in 4.6 specimen (7% of DoD) [mm].

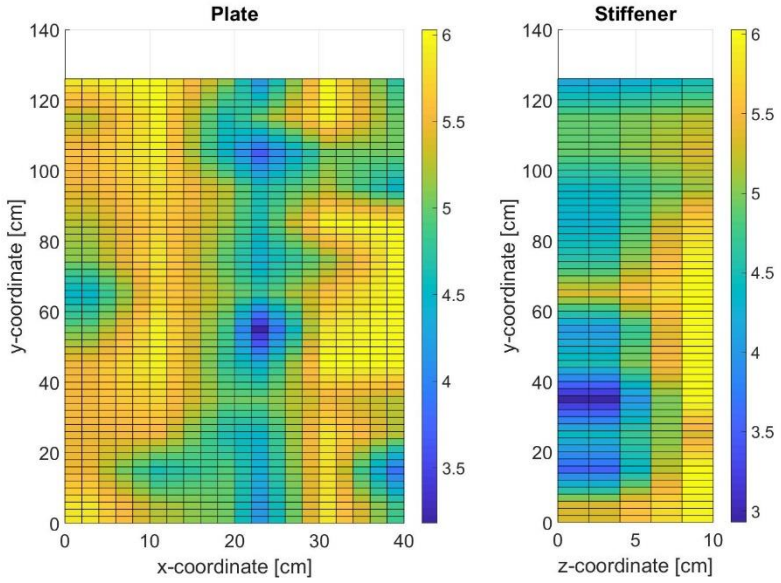


**Figure 16.** Thickness distribution in 1.6 specimen (14% of DoD) [mm].

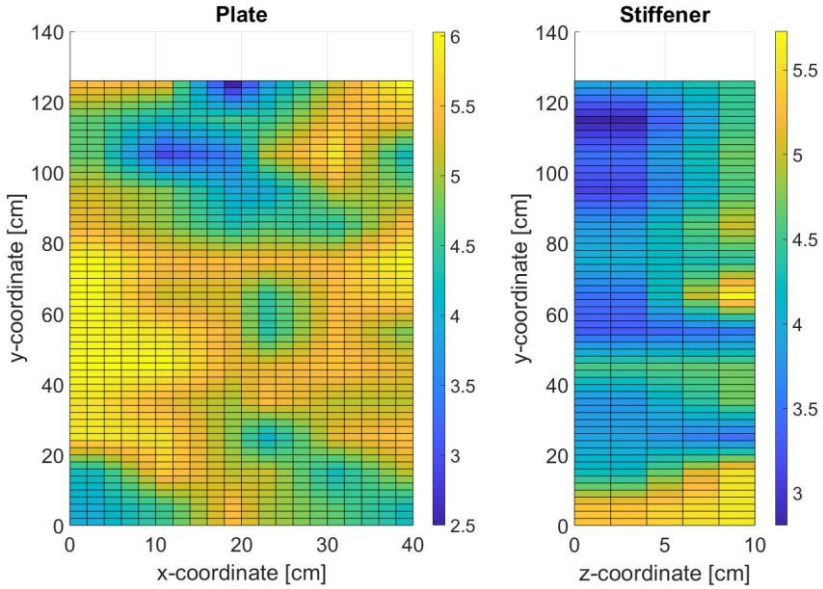


**Figure 17.** Thickness distribution in 3.6 specimen (21% of DoD) [mm].

The thickness distributions for initially 8 mm stiffened plates are presented in Figures 18 – 20. The distribution of thickness for 2.8 specimen is shown in Figure 18. It is noted that the higher corrosion diminutions for both plates and the stiffener are near the bottom and top of the specimen. In the specimen with a 14% degradation level (see Figure 19), high corrosion diminutions are observed near the plate's welding zone and right side. High corrosion depths are kept in the lower part of the stiffener, which is relatively uniformly corroded. In the most strongly corroded specimen (see Figure 20), the severely corroded regions in the plate are the bottom, top and left side. In the case of the stiffener, there is an irregular field; however, near the bottom are the highest corrosion deteriorations observed.

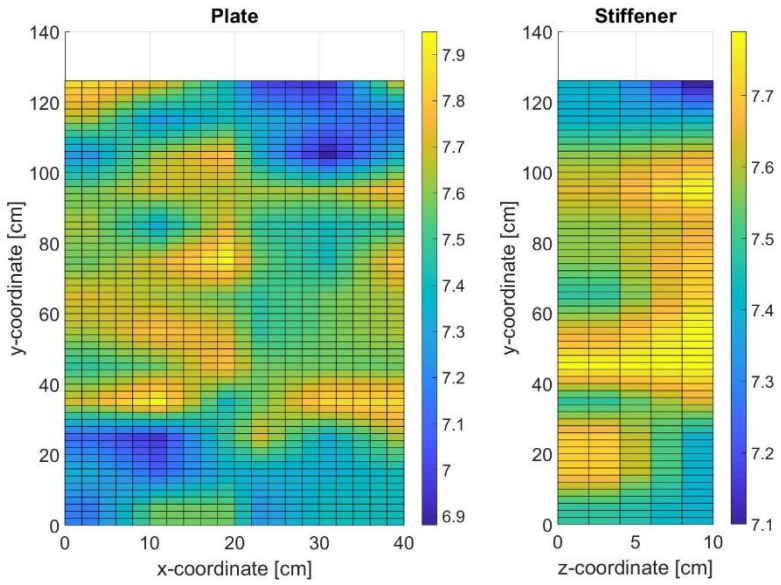


**Figure 18.** Thickness distribution in 2.8 specimen (7% of DoD) [mm].

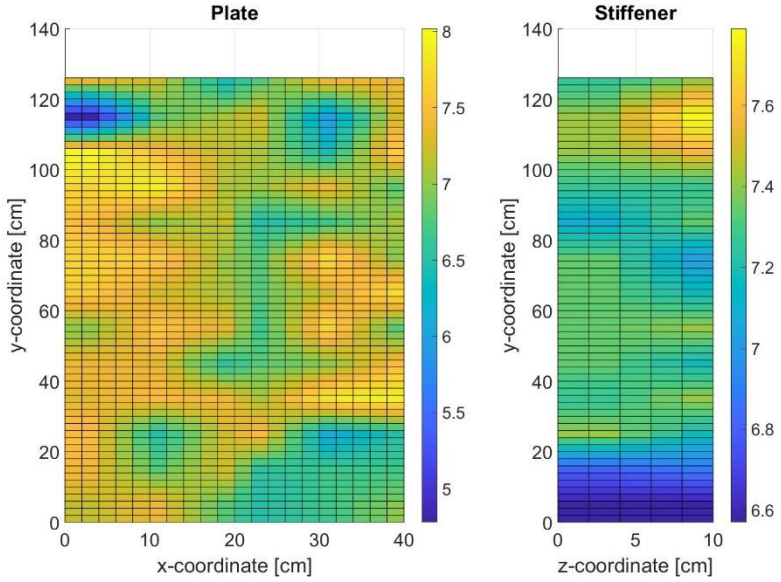


**Figure 19.** Thickness distribution in 1.8 specimen (14% of DoD) [mm].

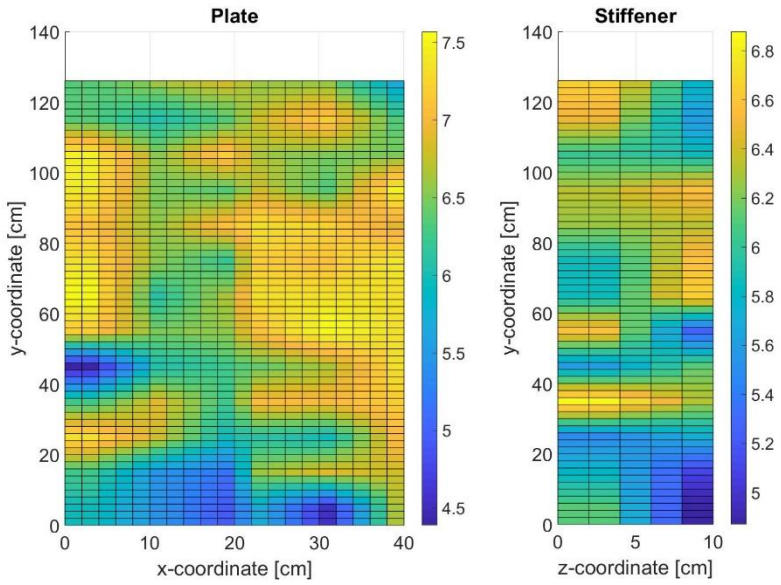


**Figure 20.** Thickness distribution in 3.8 specimen (21% of DoD) [mm].

One can capture some corrosion patterns common to most of the specimens. In general, the zone which was subjected to the highest corrosion depths was the welding region. The weld metal compositions are usually optimized to enhance their mechanical properties. This causes higher corrosion rates compared to the base metal since welded regions are more anodic. Additionally, in many specimens, both the plate and the stiffener's free edges were strongly corroded.

The statistics of the thickness for both plate and the stiffener are presented in Table 9. The mean corrosion depths for both plate and the stiffener are close to each other; for most specimens, the difference is not higher than 5% of the initial thickness. The standard deviation of thickness in the plate is more elevated for almost all cases (except specimen 1.6) than the stiffener, which is an understandable observation since it has a much higher area than the stiffener.

**Table 9.** Statistics of the thickness of large-scale specimens.

| Plate number | Mean thickness [mm] | | | Standard deviation [mm] | | |
|---|---|---|---|---|---|---|
| | Plate | Stiffener | Total | Plate | Stiffener | Total |
| 1.5 | 4.66 | 4.54 | 4.63 | 0.295 | 0.269 | 0.292 |
| 2.5 | 3.90 | 3.86 | 3.89 | 0.628 | 0.350 | 0.570 |
| 4.5 | 4.29 | 4.07 | 4.25 | 0.568 | 0.317 | 0.521 |
| 1.6 | 5.27 | 5.02 | 5.22 | 0.639 | 0.855 | 0.700 |
| 3.6 | 5.06 | 4.25 | 4.89 | 0.720 | 0.787 | 0.807 |
| 4.6 | 5.65 | 5.75 | 5.67 | 0.496 | 0.369 | 0.469 |
| 1.8 | 7.11 | 7.24 | 7.14 | 0.516 | 0.278 | 0.470 |
| 2.8 | 7.51 | 7.58 | 7.52 | 0.234 | 0.167 | 0.220 |
| 3.8 | 6.62 | 6.04 | 6.50 | 0.671 | 0.520 | 0.682 |

The estimated mean value and standard deviation of corrosion thickness in the plates are shown in Table 9. According to Garbatov et al. (2006), the standard deviation value of corrosion depth will be time-dependent and can be determined as:

$$StDev(t) = 0.384\ Ln(t + 10.54) - 0.71 \tag{5}$$

The standard deviations from Table 9 can be fitted to Eqn 5. Since the tested plates are exposed to seawater, their corrosion degradation will be like the corrosion degradation of deck plates of ballast tanks. The transition time is about 17.5 years, and the long-term corrosion depth is calibrated to obtain the same mean corrosion rate for non-accelerated conditions (0.0787 mm/year). The long-term corrosion depth is estimated at 2.36 mm. Based on Equations 1 and 5, the dependency between corrosion depth and standard deviation of plate thickness is derived, presented in Figure 21. Based on Eqn 5, the standard deviation is shown as a function of the corrosion depth and not as a function of time; thus, the relationship is linear instead of logarithmic.

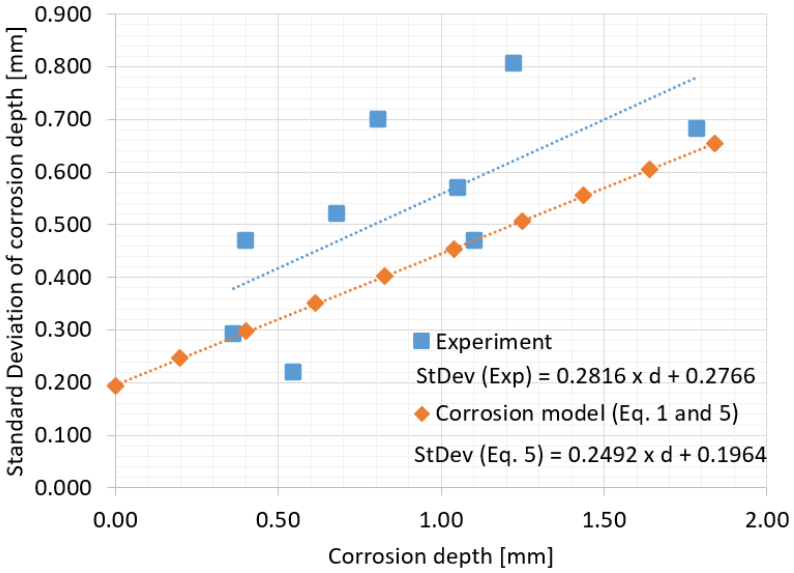


**Figure 21.** Standard deviation of corrosion depth vs corrosion depth.

It is noted that the standard deviation obtained from measurements is higher in comparison to the corrosion model. This could result from more detailed measurements in the current work, whereas the model is based on the in-situ measurements performed in real operating ships. In the latter case, not so many measuring points are captured. Nevertheless, the inclination of both curves is very similar, and there can be used for the estimation of standard deviation with corrosion development.

## 5. Conclusions

An experimental set-up for indoor accelerated controlled marine corrosion degradation of small and large-scale specimens was developed and found to be very efficient since the significant acceleration of corrosion rate and trend coinciding with a real marine corrosion degradation of deck plate of ballast and cargo tank has been achieved. Based on the assumption in the design of the set-up regarding the error and confidence level of measurements during the corrosion degradation, the initially estimated corrosion acceleration and corrosion depth have had been achieved. Some improvements to the set-up may still be implemented and possibly reduce the spread in the corrosion rate between specimens and provide improved convergence between corrosion depths in the small and large-scale specimens. Introducing additional circulation pumps was found to be very efficient in developing a multi-stage corrosion degradation. In addition, it was found that the transition time will decrease for the following stages.

The resulting thickness distribution was highly non-uniform in the small and large-scale specimens. The thickness standard deviation in stiffened plates was even higher when compared to the one obtained from the in-situ ship inspections. Additionally, higher corrosion diminutions were observed near the welding zone. In small-scale specimens, the achieved corrosion degradation fields were highly correlated. It is noted, that in the current study, both of plate surfaces were subjected to the same corrosive environment. In the case of ship structures, usually, surfaces will be subjected to different conditions. Thus, further studies in that direction should be carried out.

Similar corrosion depths, trends and scatters were achieved after 400 days of accelerated corrosion degradation, like after many years of natural corrosion degradation of deck plate of ballast and cargo tanks of tanker ships in (Garbatov et al., 2006), which was the main objective of the present work and shows that the developed experimental set-up and approach used for accelerated controlled corrosion degradation are efficient and can reproduce corrosion degraded marine structures, which can be used in the structural integrity analysis of ageing structures. Since the presented approach controls only natural factors, without application of DC current, it could be easily adapted for testing of other metallic structures or composite ones.

**Author Contributions:** Conceptualisation, KW and YG; methodology, KW and YG; formal analysis, KW; writing—original draft preparation, KW and YG; writing—review and editing, KW and YG; experimental analysis, KW and JK All authors have read and agreed to the published version of the manuscript.

**Funding:** This research was funded by The National Science Centre, Poland (grant No. 2018/31/N/ST8/02380, entitled "Experimental and numerical investigations of progressive collapse of ageing structures exposed to corrosion and locked cracks").

**Acknowledgements:** Many thanks to Prof. Juliusz Orlikowski for helping with the development of the corrosion testing set-up.

**Conflicts of Interest:** The authors declare no conflict of interest. The funders had no role in the study's design, in the collection, analyses, or interpretation of data, in the writing of the manuscript, or in the decision to publish the results.

## References

ABS, 2002. ABS Database of Corrosion Wastage for Oil Tankers, ABS RD 2002-07.

ASTM Norma G 52, 2006. Standard Practice for Exposing and Evaluating Metals and Alloys in Surface Seawater. Annu. B. ASTM Stand. https://doi.org/10.1520/G0052-00R06.2

Baboian, R., 2005. Corrosion Tests and Standards: Application and Interpretation-Second Edition, Corrosion Tests and Standards: Application and Interpretation-Second Edition. ASTM International. https://doi.org/10.1520/MNL20-2ND-EB

Bowers, P.G., Hofstetter, C., Letter, C.R., Toomey, R.T., 1995. Supersaturation Limit for Homogeneous Nucleation of Oxygen Bubbles in Water at Elevated Pressure: "Super-Henry's Law." J. Phys. Chem. 99, 9632–9637. https://doi.org/10.1021/j100023a048

Cegla, F., Gajdacsi, A., 2016. Mitigating the effects of surface morphology changes during ultrasonic wall thickness monitoring, in: AIP Conference Proceedings. p. 170001. https://doi.org/10.1063/1.4940624

Chen, H., Cui, H., He, Z., Lu, L., Huang, Y., 2021. Influence of chloride deposition rate on rust layer protectiveness and corrosion severity of mild steel in tropical coastal atmosphere. Mater. Chem. Phys. 259, 123971. https://doi.org/10.1016/j.matchemphys.2020.123971

Colt, J., Westers, H., 1982. Production of Gas Supersaturation by Aeration. Trans. Am. Fish. Soc. 111, 342–360. https://doi.org/10.1577/1548-8659(1982)111<342:POGSBA>2.0.CO;2

Dowdy, S.M., Wearden, S., Chilko, D.M., 2004. Statistics for research. Wiley-Interscience.

Garbatov, Y., Guedes Soares, C., 2007. Structural Reliability of Ship Hull Subjected to Nonlinear Time Dependent Deterioration, Inspection and Repair, in: 10th International Symposium on Practical Design of Ships and Other Floating Structures. American Bureau of Shipping, Huston, Texas, United States of America.

Garbatov, Y., Guedes Soares, C., Wang, G., 2007. Nonlinear Time Dependent Corrosion Wastage of Deck Plates

of Ballast and Cargo Tanks of Tankers. J. Offshore Mech. Arct. Eng. 129, 48–55. https://doi.org/10.1115/1.2426987

Garbatov, Y., Guedes Soares, C., Wang, G., 2006. Nonlinear Time Dependent Corrosion Wastage of Deck Plates of Ballast and Cargo Tanks of Tankers. J. Offshore Mech. Arct. Eng. 129, 48–55. https://doi.org/10.1115/1.2426987

Garbatov, Y., Saad-Eldeen, S., Guedes Soares, C., Parunov, J., Kodvanj, J., 2018. Tensile test analysis of corroded cleaned aged steel specimens. Corros. Eng. Sci. Technol. 1–9. https://doi.org/10.1080/1478422X.2018.1548098

Garbatov, Y., Tekgoz, M., Guedes Soares, C., 2017. Experimental and numerical strength assessment of stiffened plates subjected to severe non-uniform corrosion degradation and compressive load. Ships Offshore Struct. 12, 461–473. https://doi.org/10.1080/17445302.2016.1173807

Guedes Soares, C., Garbatov, Y., 1999. Reliability of maintained, corrosion protected plates subjected to non-linear corrosion and compressive loads. Mar. Struct. 12, 425–445. https://doi.org/10.1016/S0951-8339(99)00028-3

Guedes Soares, C., Garbatov, Y., 1998. Non-linear time dependent model of corrosion for the reliability assessment of maintained structural components. A. A. Balkema, Saf. Reliab. 2, 929–936.

ISO, 2009. Metallic materials - Tensile testing - Part 1: Method of test at room temperature. Int. Stand. ISO 6892-1.

Jin, Y.-H., Ha, M.-G., Jeon, S.H., Jeong, Y.-S., Ahn, J.-H., 2020. Evaluation of corrosion conditions for the steel box members by corrosion monitoring exposure test. Constr. Build. Mater. 258, 120195. https://doi.org/10.1016/j.conbuildmat.2020.120195

Melchers, R.E., 2008. Development of new applied models for steel corrosion in marine applications including shipping. Ships Offshore Struct. 3, 135–144. https://doi.org/10.1080/17445300701799851

Melchers, R.E., 1999. Corrosion uncertainty modelling for steel structures. J. Constr. Steel Res. 52, 3–19. https://doi.org/10.1016/S0143-974X(99)00010-3

Nie, B., Xu, S., Yu, J., Zhang, H., 2019. Experimental investigation of mechanical properties of corroded cold-formed steels. J. Constr. Steel Res. 162, 105706. https://doi.org/10.1016/j.jcsr.2019.105706

Orlikowski, J., Jazdzewska, A., Mazur, R., Darowicki, K., 2017. Determination of pitting corrosion stage of stainless steel by galvanodynamic impedance spectroscopy. Electrochim. Acta 253, 403–412. https://doi.org/10.1016/j.electacta.2017.09.047

P. Domzalicki, I. Skalski, C. Guedes Soares, Y.G., 2009. Large Scale Corrosion Tests, in: P.K. Das (Ed.), Analysis and Design of Marine Structures. Taylor & Francis Group, pp. 193–198.

Paik, J.K., Kim, S.K., Lee, S.K., 1998. Probabilistic corrosion rate estimation model for longitudinal strength members of bulk carriers. Ocean Eng. 25, 837–860. https://doi.org/10.1016/S0029-8018(97)10009-9

Pedeferri, P., 2018. Corrosion Science and Engineering, Engineering Materials. Springer International Publishing, Cham. https://doi.org/10.1007/978-3-319-97625-9

Qin, S., Cui, W., 2003. Effect of corrosion models on the time-dependent reliability of steel plated elements. Mar. Struct. 16, 15–34. https://doi.org/10.1016/S0951-8339(02)00028-X

Saad-Eldeen, S., Garbatov, Y., Guedes Soares, C., 2013. Experimental assessment of corroded steel box-girders

subjected to uniform bending. Ships Offshore Struct. 8, 653–662. https://doi.org/10.1080/17445302.2012.718171

Toloei, A., Stoilov, V., Northwood, D., 2013. The Relationship Between Surface Roughness and Corrosion, in: Volume 2B: Advanced Manufacturing. American Society of Mechanical Engineers. https://doi.org/10.1115/IMECE2013-65498

Wang, G., Spencer, J., Elsayed, T., 2003. Estimation of Corrosion Rates of Oil Tankers, in: Proceedings of the 22nd International Conference on Offshore Mechanics and Arctic Engineering. ASME Paper No. OMAE 2003-37361, Cancun, Mexico.

Wang, X., Moan, T., 1996. Stochastic and deterministic combinations of still water and wave bending moments in ships. Mar. Struct. 9, 787–810. https://doi.org/10.1016/0951-8339(95)00022-4

Wang, Y., Xu, S., Li, A., 2020. Flexural performance evaluation of corroded steel beams based on 3D corrosion morphology. Struct. Infrastruct. Eng. 1–16. https://doi.org/10.1080/15732479.2020.1713169

Woloszyk, K., Garbatov, Y., 2021. Accelerated large scale test set-up design in natural corrosion marine environment, in: Guedes Soares, C., Santos, T.A. (Eds.), Developments in Maritime Technology and Engineering. CRC Press, London, pp. 517–524. https://doi.org/10.1201/9781003216582-58

Woloszyk, K., Garbatov, Y., Kowalski, J., Samson, L., 2020. Experimental and numerical investigations of ultimate strength of imperfect stiffened plates of different slenderness. Polish Marit. Res. 27, 120–129.

Xiao, L., Peng, J., Zhang, J., Ma, Y., Cai, C.S., 2020. Comparative assessment of mechanical properties of HPS between electrochemical corrosion and spray corrosion. Constr. Build. Mater. 237, 117735. https://doi.org/10.1016/j.conbuildmat.2019.117735

Xu, S., Zhang, H., Wang, Y., 2019. Estimation of the properties of corroded steel plates exposed to salt-spray atmosphere. Corros. Eng. Sci. Technol. 54, 431–443. https://doi.org/10.1080/1478422X.2019.1613779

Yamamoto, N., Ikegami, K., 1998. A Study on the Degradation of Coating and Corrosion of Ship's Hull Based on the Probabilistic Approach. J. Offshore Mech. Arct. Eng. 120, 121–128. https://doi.org/10.1115/1.2829532

Yamashita, T., Ando, K., 2017. Aeration of water with oxygen microbubbles and its purging effect. J. Fluid Mech. 825, 16–28. https://doi.org/10.1017/jfm.2017.376

Yuan, Y., Ji, Y., Shah, S., 2007. Comparison of Two Accelerated Corrosion Techniques for Concrete Structures. ACI Struct. J. 104, 344–347. https://doi.org/10.14359/18624

Zakowski, K., Narozny, M., Szocinski, M., Darowicki, K., 2014. Influence of water salinity on corrosion risk—the case of the southern Baltic Sea coast. Environ. Monit. Assess. 186, 4871–4879. https://doi.org/10.1007/s10661-014-3744-3

Zhu, J., Li, D., Chang, W., Wang, Z., Hu, L., Zhang, Y., Wang, M., Yang, Z., Song, J., Chen, S., Zhang, Liang, Zhang, Lei, 2020. In situ marine exposure study on corrosion behaviors of five alloys in coastal waters of western Pacific Ocean. J. Mater. Res. Technol. 9, 8104–8116. https://doi.org/10.1016/j.jmrt.2020.05.060